Video Article

Novel Techniques for Observing Structural Dynamics of Photoresponsive Liquid Crystals

Masaki Hada[1], Shohei Saito[2], Ryuma Sato[3], Kiyoshi Miyata[4], Yasuhiko Hayashi[1], Yasuteru Shigeta[3], Ken Onda[4]

[1]Graduate School of Natural Science and Technology, Okayama University

[2]Graduate School of Science, Kyoto University

[3]Center for Computational Sciences, University of Tsukuba

[4]Graduate School of Science, Kyushu University

Correspondence to: Masaki Hada at hadamasaki@okayama-u.ac.jp, Ken Onda at konda@chem.kyushu-univ.jp

URL: https://www.jove.com/video/57612
DOI: doi:10.3791/57612

Keywords: Chemistry, Issue 135, Time-resolved electron diffraction, time-resolved infrared vibrational spectroscopy, structural dynamics, femtosecond laser, ultrafast phenomena, liquid crystals

Date Published: 5/29/2018

Citation: Hada, M., Saito, S., Sato, R., Miyata, K., Hayashi, Y., Shigeta, Y., Onda, K. Novel Techniques for Observing Structural Dynamics of Photoresponsive Liquid Crystals. *J. Vis. Exp.* (135), e57612, doi:10.3791/57612 (2018).

Abstract

We discuss in this article the experimental measurements of the molecules in liquid crystal (LC) phase using the time-resolved infrared (IR) vibrational spectroscopy and time-resolved electron diffraction. Liquid crystal phase is an important state of matter that exists between the solid and liquid phases and it is common in natural systems as well as in organic electronics. Liquid crystals are orientationally ordered but loosely packed, and therefore, the internal conformations and alignments of the molecular components of LCs can be modified by external stimuli. Although advanced time-resolved diffraction techniques have revealed picosecond-scale molecular dynamics of single crystals and polycrystals, direct observations of packing structures and ultrafast dynamics of soft materials have been hampered by blurry diffraction patterns. Here, we report time-resolved IR vibrational spectroscopy and electron diffractometry to acquire ultrafast snapshots of a columnar LC material bearing a photoactive core moiety. Differential-detection analyses of the combination of time-resolved IR vibrational spectroscopy and electron diffraction are powerful tools for characterizing structures and photoinduced dynamics of soft materials.

Video Link

The video component of this article can be found at https://www.jove.com/video/57612/

Introduction

Liquid crystals (LCs) have a variety of functions and are widely used in scientific and technological applications[1,2,3,4,5,6]. The behavior of LCs can be attributed to their orientational ordering as well as to the high mobility of their molecules. A molecular structure of LC materials is typically characterized by a mesogen core and long flexible carbon chains that ensure high mobility of the LC molecules. Under external stimuli[7,8,9,10,11,12,13,14,15], such as light, electric fields, temperature changes, or mechanical pressure, small intra- and intermolecular motions of the LC molecules cause drastic structural reordering in the system, leading to its functional behavior. To understand the functions of LC materials, it is important to determine the molecular scale structure in the LC phase and identify the key motions of the molecular conformations and packing deformations.

X-ray diffraction (XRD) is commonly employed as a powerful tool for determining structures of LC materials[16,17,18]. However, the diffraction pattern originating from a functional stimuli-responsive core is often concealed by a broad halo pattern from the long carbon chains. An effective solution to this problem is provided by time-resolved diffraction analysis, which enables direct observations of molecular dynamics using photoexcitation. This technique extracts structural information about the photoresponsive aromatic moiety using the differences between the diffraction patterns obtained before and after photoexcitation. These differences provide the means both to remove the background noise and to directly observe the structural changes of interest. Analyses of the differential diffraction patterns reveal the modulated signals from the photoactive moiety alone, thereby excluding the deleterious diffraction from the non-photoresponsive carbon chains. A description of this method of differential diffraction analysis is provided in Hada, M. *et al*[19].

Time-resolved diffraction measurements can provide structural information about the atomic rearrangements that occur during the phase transition in materials[20,21,22,23,24,25,26,27,28,29] and chemical reactions among molecules[30,31,32,33,34]. With these applications in mind, remarkable progress has been made in the development of ultrabright and ultrashort-pulsed X-ray[35,36] and electron[37,38,39,40] sources. However, time-resolved diffraction has only been applied to simple, isolated molecules or to single- or poly-crystals, in which highly ordered inorganic lattice or organic molecules produce well-resolved diffraction patterns providing structural information. In contrast, ultrafast structural analyses of more complex soft materials have been hampered because of their less ordered phases. In this study, we demonstrate the use of time-resolved electron diffraction as well as transient absorption spectroscopy and time-resolved infrared (IR) vibrational spectroscopy to characterize the structural dynamics of photoactive LC materials using this diffraction-extracted methodology[19].

Protocol

1.Time-Resolved Infrared Vibrational Spectroscopy

1. **Sample preparation**
   1. Solution: Dissolve the π-extended cyclooctatetraene (π-COT) molecules into dichloromethane with proper concentration (1 mmol/L).
   2. LC phase: Melt the π-COT powder on a calcium fluoride (CaF_2) substrate using hot plate at the temperature of 100 °C. Cool the sample at a room temperature.
      Note: We need to choose a material (CaF_2 or barium fluoride (BaF_2)) that is transparent in mid-IR range.

2. **Apparatus setting-up**
   1. Switch on the titanium sapphire (Ti:sapphire) laser and the chirped pulse amplifier. Thermally stabilize them for several hours.
   2. Make sure the alignments are correct. Check the power and stability of the ultraviolet (UV) pump and the mid-IR probe and re-align the optical path if necessary. The optical setup of the time-resolved infrared spectroscopy is provided in **Figure 5**.
   3. Cool the HgCdTe IR detector array using liquid nitrogen. Make sure that the spectrometer is properly located so that reasonable amount of light is detected in the range of interest. Calibrate the spectrometer using absorption spectra of well-known materials such as polystyrene or polyethylene terephthalate.
   4. Mount a sample which shows large photo-induced transient response (Si wafer (1 mm) or $Re(bpy)(CO)_3Cl/CH_3CN$ solution) on the sample holder. Locate the pump-probe delay to a positive value and optimize the amount of the transient signal by stirring the pump beam to ensure the pump-probe overlap.
   5. Find the time origin setting by taking long-range scan on the pump-probe delay using the home-built program (**Figure 6**). Check the position where the transient signal start to emerge.
   6. Check the dynamics of symmetric and anti-symmetric vibration of CO stretching in $Re(bpy)(CO)_3Cl$ whose dipole moments are orthogonal. Note that both should show exactly same dynamics when the magic angle condition is properly met.

3. **Measurement and data acquisition**
   1. Solution: Mount the home-built flow cell. Setup the bubbling device with inert gas (nitrogen (N_2) or Argon (Ar)) if necessary. LC phase: Mount the spin-coated π-COT sample with the substrate on the motorized stage to continuously move the laser spots on the sample to minimize the laser-induced damage.
   2. Doublecheck the time zero position with the sample.
   3. Set the scan range of the pump-probe delay properly (start, end, and step).
   4. Choose a directory to save data.
   5. Start the data collection with the home-built program.
      NOTE: The data are recorded automatically in the directory.

2. Time-Resolved Electron Diffraction

1. **Fabrication of sample substrate**
   1. Purchase a silicon (001) wafer (200 μm thick), both sides of which are pre-covered with 30-nm-thick silicon-rich silicon nitride (Si_3N_4, or simply SiN) film (**Figure 11A**). Cut the SiN/Si/SiN wafer in square (15 × 15 mm^2).
   2. Irradiate with Ar cluster ion beams[41] at the fluence of 2.5 × 10^{16} ions/cm^2 onto one of the sides of the SiN/Si/SiN wafer though a metal mask (**Figure 12**), which is sufficient to remove the 30-nm-thick SiN film (**Figure 11B,C**).
      NOTE: An alternative method to remove SiN film is plasma etching or ion beams etching.
   3. Prepare potassium hydroxide (KOH)aqueous solution at a concentration of 28%.
   4. Put the wafer into KOH solution at a temperature of 60-70 °C for 1-2 days (**Figure 11D**), which perform further etching of the Si wafer via isotropic chemical etching[42].
      NOTE: The etching rate for Si by KOH solution is much faster than that for SiN, so the SiN thin film remains as self-supporting membranes (**Figure 11E**).
   5. Clean the wafer with SiN membranes in deionized water and dry it with nitrogen gas.

2. **Sample preparation**
   1. Dissolve the π-COT molecules in chloroform at a concentration of 10 mg/mL.
   2. Program the spin-coater: accelerate to 2000 rpm in 5 s, keep the rotation for 30 s, and stop the rotation. Spin-coat the π-COT solution onto the SiN membrane substrate as shown in **Figure 11F**.
      NOTE: A proper wafer size for spin-coating must be more than 10 × 10 mm^2, since the surface tension sometimes interferes with spin-coating of materials on smaller wafers, for example, a SiN membrane grid for transmission electron microscopy.
   3. Put the sample coated on the SiN membrane substrate on a hotplate at a temperature of 100 °C, melt it, and cool it gradually to room temperature (**Figure 11G**).

3. **Measurements**
   1. Mount the sample on the sample holder with a screw and put the sample holder in the vacuum chamber (sample chamber).
   2. Seal the vacuum chamber with a lid and switch on a rotary pump to evacuate the chamber until a vacuum level of less than 1000 Pa. Then, switch on the molecular turbo pumps until the electron-gun chamber is at the vacuum level of ~10^{-6} Pa (typically for more than 12 h).
   3. Switch on the Ti:sapphire laser and the chirp pulse amplifier, and thermally stabilize them for more than 1 h. The experimental setup of the time-resolved electron diffraction is provided in **Figure 9**. Set the repetition rate to 500 Hz.

4. Switch on the thriller of the charge-coupled device (CCD) camera and cool it to 10 °C.
5. Switch on the electrical power supply and adjust the voltage to 75 kV.
   NOTE: The leak current of the power supply should not fluctuate out of the 0.1 μA range.
6. Special overlap. Open the laboratory-coded automatic program (**Figure 10A**) and set the exposure time (50 ms). Find the electron beam position with a pinhole equipped in the sample holder using the program by setting **Start type** to **Z_overlap** for the overlap of Z-axis and Y_overlap and pressing **Start** button.
7. Set the electron beam at the pinhole position and align the pump laser with the reflected pump light by the pinhole.
8. Measure the time-zero position with an inorganic material (Bi_2Te_3) on the sample holder using a laboratory-coded automatic program (**Figure 10B**) by setting **Start type** to Time-resolved and pressing Start button. For this process, adjust the pump fluence to 2 mJ/cm^2.
9. Insert the Faraday cup to the pass of the electron beam and measure the fluence of the electron beam with a laboratory-built picoammeter and adjust it by rotating the adjustable ND filter on the probe line. Adjust thefluence of the pump pulse by rotating the waveplate on the pump line.
10. Move to the sample position and set the exposure time of the CCD camera. Obtain the electron diffraction image using the laboratory-coded automatic program (**Figure 10B**) by setting **Start type** to **Single** and pressing **Start** button.
11. Switch on the Peltier element of the CCD camera and cool it down to the temperature of -20 °C.
12. Set the time-step and number of steps for the time-resolved measurements. Obtain the time-resolved electron diffraction images using the laboratory-coded automatic program (**Figure 10B**) by setting **Start type** to **Time-resolved** and pressing **Start** button.
13. Obtain the time-resolved background image with the electron acceleration power supply switching off using the laboratory-coded automatic program (**Figure 10B**) by setting **Start type** to **Time-resolved** and pressing **Start** button.

Representative Results

We chose a saddle-shaped π-COT skeleton[43,44] as a photoactive core unit of the LC molecule, because it forms a well-defined columnar stacking structure and because the central eight-membered COT ring is expected to show a photoinduced conformational change into a flat form owing to the excited-state aromaticity[19,45]. Synthetic process of this material is provided in previous publication[19]. The synthesized LC molecule is composed of a π-COT core unit and a typical dendritic carbon chain moiety[46,47], with the molecular formula of $C_{204}H_{324}N_4O_{12}S_4$ (**Figure 1**). The material exhibits a columnar LC phase at room temperature, which enabled the structural analysis of the LC phase to be performed without controlling the temperature. **Figure 2** shows the XRD pattern of the LC phase obtained using Cu Kα radiation. In the spectrum, several peaks show up at low diffraction angles ($2\theta < 10°$; $d > 8.8$ Å), along with a broad peak at a wide diffraction angle ($2\theta \approx 20°$; $d \approx 4.4$ Å). The LC structure is characterized as a rectangular columnar form, in which saddle molecules align on top of one another. The XRD analysis yielded the lattice parameters of a = 62 Å and b = 42 Å. The intermolecular distance in the stacked column along the *c*-axis was obscured by a broad diffraction peak originating from the dendritic carbon chain moiety. This situation is quite common for typical columnar LC materials.

The photoinduced dynamics of the columnar LC material consist of a sequence of structural motions on different timescale. First, a conformational change occurs at the molecular level. This is followed by deformations of the local packing structure that take place around the photoexcited molecules in the π-stacked columns. We first performed transient transmission spectroscopy with various pump and probe energies on thin films of the π-COT molecule, to confirm the optical excitation and associated photoinduced dynamics. Transient absorption spectroscopy is the conventional type of time-resolved spectroscopy, which is commercially available these days. A 100 fs optical pulse from a chirped-pulse amplifier is separated into pump and probe beams. The pulse in the pump beam (pump pulse) at a wavelength of 800 nm is converted into photons of 266 nm wavelength by two beta barium borate (BBO) crystals. The pulse in the probe beam (probe pulse) is focused through a sapphire window to generate white light (500-700 nm). The two optical pulses are focused onto the sample using fused-silica lenses, and the transmitted white probe beam is dispersed by the spectrometer and detected with a Si photodiode. The incident fluence of the pump beam used in our experiments was 1 mJ/cm^2. The sample was spread onto a substrate of bulk CaF_2, melted at 100°C on a hot plate, and then cooled gradually to room temperature. The bulk BaF_2 and CaF_2 substrates are transparent over the wavelength range from 150 nm to 12 μm and 130 nm to 10 μm, respectively. The measurable wavelength range of these materials depends on the thickness of sample and substrate as well as the intensity of IR light.

Figure 3A shows the transient visible transmittance at pump and probe energies of 4.7 eV and approximately 2.1 eV (wavelengths of 266 and 500-700 nm), respectively. A molecule that absorbs UV light is immediately excited to a far-from-equilibrium state (S_n) and transfers to the S_1 state within 2 ps, as shown in **Figure 3B**. Once in the S_1 or T_1 state, the molecule returns to the S_0 state in 20 or 150 ps (**Figure 4**). However, a small proportion of the molecules remains in the excited state for over 1 ns. We fitted the transient transmittance with the following equation:

$$\Delta T/T = A_1 \exp(-t/\tau_1) + A_2 \exp(-t/\tau_2) + A_3, \quad (1)$$

where the first and second terms indicate exponential decay with the time-constants of τ_1 = 20 ps and τ_2 = 150 ps. The third term suggests the decay of even longer timescale (>500 ps).

To confirm the photoinduced conformational change, we performed time-resolved IR vibrational spectroscopy on the π-COT thin film in the LC phase.The experimental setup of UV pump at the wavelength of 266 nm and mid-infrared (IR) probe at the wavelength of 1050-1700 cm^{-1} time-resolved IR vibrational spectroscopy[48,49,50,51] is shown in **Figure 5**. The graphical user interface of the laboratory-coded automatic program is shown in **Figure 6**. The measurements were performed in the transmission mode for π-COT molecules in solution (1 mmol/L in CH_2Cl_2 solvent) and for the LC phase coated on a CaF_2 substrate. A near-IR optical pulse (800 nm), with a pulse duration of 120 fs, was separated into pump and probe beams with a beam splitter. The pump pulse was converted into a UV (266 nm) pulse by means of two BBO crystals and a calcite crystal. One beam of the probe pulse was converted to mid-IR wavelength (1000-4000 cm^{-1}) by using an optical parametric amplifier equipped with a difference-frequency-generation crystal, $AgGaS_2$. The UV pump and mid-IR probe pulses were focused on the sample with lenses. The angle of incidence of the pump and probe beams were set to be approximately perpendicular to the surface of the sample. The repetition rate and the incident fluence of the UV pump pulse were 500 Hz and 1 mJ/cm^2, respectively. The broad-bandwidth probe pulse was dispersed by a grating and then acquired by a 64-channel, HgCdTe IR detector array. The ultrafast electronic response of silicon was used to determine "time-zero"[52] when the pump and probe pulses arrive simultaneously at the sample position. Different types of sample holders were used to measure the samples in solution and in the LC phase. The LC coated on CaF_2 substrate was held by a clamp on a simple optical holder mounted on a motorized state. The motorized stage moved the sample relative to the laser focusing spot incoherently with the pump-probe measurements to minimize the laser-induced damage. In contrast, the sample in solution was introduced into a laboratory-built liquid-flow cell equipped with two BaF_2 windows, with an optical path length of 100 μm through the sample. The liquid-flow cell is a closed-loop system supplied by a diaphragm pump.

The observed IR-active modes in the saddle and flat structures were assigned according to density-functional-theory (DFT) frequency calculations. Details of the DFT calculations are provided in the main text and in the supplementary materials of a previous publication[19]. The resulting time-resolved spectra display the evolution of the molecular vibrational modes of the planar π-COT unit. **Figure 7** shows the differential vibrational spectrum at a delay time of 100 ps, along with the calculated T_1-S_0 differential vibrational spectrum, which was obtained by subtracting the spectrum of the saddle form in S_0 from the spectrum at the flat form in T_1. The figure shows that the experimental data and the calculations are broadly in agreement with each other. Better agreement was obtained with the T_1-S_0 spectrum than with the S_1-S_0 spectrum, although both the S_1 and T_1 optimized structures exhibited similar flat conformations. After the photoexcitation, we observed several peaks in the vibrational spectra. The characteristic peaks at the wavenumbers of 1183, 1338 and 1489 cm^{-1} correspond to the stretching modes of the COT and thiazole rings or of the biphenyl moieties, which are weakly or non-IR-active in the saddle form in S_0 but strongly-IR-active in the flat form in T_1. The time-dependent evolution of the peak intensity at 1338 cm^{-1} reveals dynamics identical to those observed using transient visible transmission spectroscopy. Thus, the photoinduced dynamics at the molecular level are characterized by a saddle-to-flat conformational change of the π-COT unit within 2 ps, followed by relaxation back to the initial saddle form in 10-20 ps or 150 ps (**Figure 8A**). The time-resolved IR spectra were also fitted with Eq. (1). According to the time-evolution of the IR peak intensity (1335 cm^{-1}) from the π-COT in solution (**Figure 8B**), only the fast time-constant (10-20 ps) was observed. Therefore, the fast time-constant observed in **Figure 3B** and **Figure 8B** corresponds to the relaxation dynamics of isolated molecules, which are generally located at the surface or the interface of LC materials.

To examine packing deformation at the locations of the photoexcited molecules in the condensed LC phase, we performed time-resolved electron diffraction measurements.The experimental setup employed for compact, direct-current (DC) accelerated electron diffraction measurements[53,54] is shown in **Figure 9**. The graphical user interfaces of the laboratory-coded automatic programs are shown in **Figure 10**. The process of the sample preparation is summarized in **Figure 11**, and the sample film thickness was determined with single-wavelength (635 nm) ellipsometer to be ~100 nm, where the methodology is provided in Hada, M. *et al*.[55]. The detail of the metal mask used for the cluster ion beam irradiation is provided in **Figure 12**.

A near-IR optical pulse (800 nm) with the pulse duration of 120 fs was separated with a beam splitter into two beams: pump beam and probe beam. The near-IR pulse in the pump beam was converted into UV (266 nm) pulse using second-harmonic generation (SHG) in a BBO crystal followed by a calcite crystal, and by another BBO crystal for third-harmonic generation (THG). The calcite crystal is used to adjust the arrival time of the fundamental light and the SHG light so that they arrive simultaneously at the second BBO crystal for THG. The pump pulse is focused by a fused silica lens to photoexcite the ~100 nm thick film of π-COT molecule in the LC phase. The near-IR pulse in the probe beam was likewise converted into a UV pulse and was focused onto a gold photocathode to generate an electron pulse. The UV pulse used to generate electrons was stretched by a 25 mm thick fused-silica plate to a duration of >500 fs. The vacuum chamber used for time-resolved electron diffraction was separated in two parts, *i.e.*, the gun chamber and sample chamber. The photocathode and electrode were placed in the electron-gun chamber at a vacuum level of ~10^{-6} Pa, and the sample was placed in the sample chamber at a vacuum level of ~10^{-4} Pa. The electron pulse was accelerated to an energy of 75 keV by a DC field. The electrons that were diffracted and directly transmitted through the sample were focused with a magnetic lens onto a 1:2 fiber-coupled CCD camera coated with a P43 (Gd_2O_2S:Tb) phosphor scintillator. The time delay between the pump and probe pulses was varied by an optical state in the pump beam.

The spot sizes of the pump UV pulse and probe electron pulse was measured to be 210 and 100 μm, respectively, using a knife edge. The incident laser fluence was 1.2 mJ/cm^2. From the transmission and reflectivity of the sample-measured to be 40% and 30%, respectively, the absorption fluence was determined to be 0.36 mJ/cm^2. Photoinduced structural changes inside the material were investigated with electron pulses containing 2 × 10^4 electrons (3 fC). The time-zero was determined from the ultrafast-atomic response of an inorganic material (Bi_2Te_3)[56]. The pulse duration of the electron beam was determined to be on the order of 1 ps by a plasma method[57]. The relation between the *Q*-value and the pixel size in the CCD camera was also calibrated using the (110) and (300) diffraction spots from Bi_2Te_3. To acquire one electron-diffraction image, 1 × 10^4 electron pulses were collected at a repetition rate of 500 Hz. The quality of the SiN membrane is determined by its electron diffraction pattern, *i.e.*, the electron diffraction pattern cannot be observed from the SiN membrane because it is amorphous (**Figure 13A**).

The two-dimensional electron diffraction patterns from the LC thin film showed an ill-defined, broad halo ring originating from the long carbon chains (**Figure 13B**), similar to the wide XRD peak observed at the diffraction angle $2\theta \approx 20°$. This broad halo, which is typically observed in LC materials, is composed of a number of diffraction peaks produced by the long carbon chains and a few peaks originating from the functional core moiety (**Figure 14**). Under external stimuli, such as photoirradiation, structural deformations are induced around the stimuli-responsive core moieties, and modulation of the peak in the diffraction pattern occurs subsequently. By subtracting the initial diffraction pattern from that obtained 500 ps after UV pulse irradiation, we can extract the modulated diffraction pattern induced by the UV irradiation. The resulting differential diffraction pattern is well defined, with clearly observable negative and positive rings (**Figure 13C**), in spite of small amounts of peak modulation. The negative peaks from the original structure disappear upon photoirradiation, while the positive peaks indicate the formation of the new ordered structure.

The radial averages of the differential diffraction patterns at -50 and 500 ps after the UV pulse irradiation are presented in **Figure 15A**. Negative peaks are observed to develop at *Q*-values of 0.245 $Å^{-1}$ and 0.270 $Å^{-1}$. Using molecular dynamics (MD) simulations, we calculated the differential electron diffraction pattern shown in **Figure 15B**. The details of the MD calculations are provided in the main text and supplementary materials of reference 19. Fitting of the experimental data to the MD simulations suggests that, before photoexcitation, the structure had periodic lengths of 4.55 Å and 3.7 Å corresponding to the periodicity of the π-COT molecules along the c-axis and to the distance between the π-stacked biphenyl units, respectively. It is also worth mentioning that the corresponding dynamics is observed using time-resolved electron diffraction. The time-evolution of the intensities of the negative and positive diffraction peaks is shown in **Figure 16**. The destruction of the π-π stacking order occurs on a timescale of 300 ps and is slower than the saddle-to-flat conformational change of the molecular framework. The positive peak (at 0.37 $Å^{-1}$) starts to increase 200 ps after the photoexcitation.

For further interpretation of the time-resolved spectroscopy and diffraction, the photoexcitation level of the sample must be addressed. Using the number of incident photons (1.2 mJ/cm^2) and the number of molecules per unit area, we calculated that approximately 25% of the molecules absorb UV light and potentially undergo the saddle-to-flat conformational change. As shown by transient transmission spectroscopy and time-resolved IR vibrational spectroscopy, most photoexcited molecules relaxed to the initial state in 150 ps, but some molecules exhibited rather slow dynamics in the LC phase. In particular, 7-8% of the photoexcited molecules, at most 2% of all the molecules in the material, remained in the flat conformation for 300-1000 ps. Thus, these photoexcited flattened molecules were sandwiched between unexcited saddle-shaped molecules. To explore the subsequent packing deformations in the stacked column, we performed further MD calculations, considering five stacked molecules arranged with the order of saddle-saddle-flat-saddle-saddle conformers. In the columnar structure, the saddle-to-flat conformational change of a photoexcited molecule induces significant steric repulsion against the rigid biphenyl parts of the neighboring molecules. To avoid the steric hindrance, local structural deformations triggered twisting motions in the stacked molecules on a timescale of ~300 ps.

In **Figure 17**, we summarize our findings for the photoinduced dynamics of the π-COT molecules. The UV-photoexcitation triggers a saddle-to-flat conformational change within a few picoseconds into T_1 or S_1 of the photoresponsive core. Most of the flat-shaped, electronically excited molecules relax to their original forms within 20 ps (for isolated molecules) or 150 ps (for stacked molecules). However, a small percentage remain in the LC phase, sandwiched between the saddle-shaped molecules. Owing to the steric effects among the differently shaped molecules in the columnar packing structure, twisting motions occur within 300 ps, destroying the local stacking structure and constructing a new periodicity.

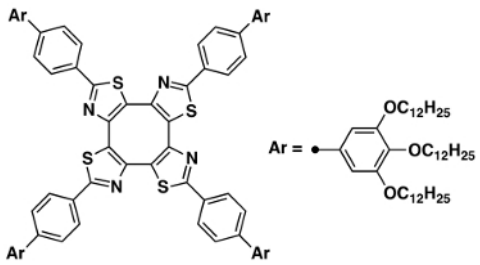

Figure 1: **Chemical structure of the π-COT-based LC molecule.** The molecular formula of the π-COT-based LC molecule is $C_{204}H_{324}N_4O_{12}S_4$ with a molecular weight of 3153.03. Please click here to view a larger version of this figure.

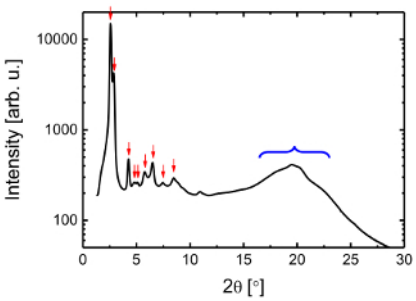

Figure 2: **The static XRD spectrum.** The X-ray diffraction pattern displays several peaks, as indicated by the red arrows. The peak assignment of those indicated by red arrows are shown in the supplementary materials of Hada, M. *et al*.[19]. The blue blanket indicates the (001) peak of the π-COT molecule. Please click here to view a larger version of this figure.

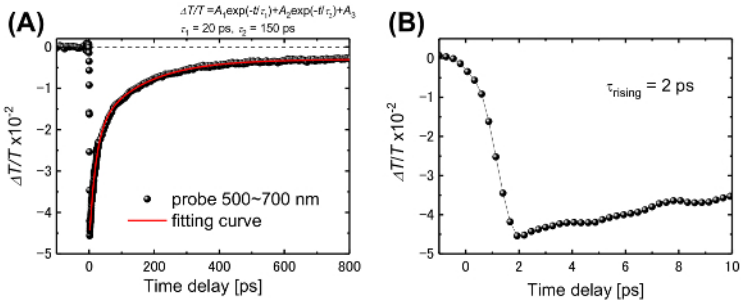

Figure 3: Time evolution of the transient transmission spectrum. (A) The rising signal component has a time-constant of 2 ps, and **(B)** the relaxation time-constants are 20 and 150 ps**.** This figure has been adapted from Hada, M. *et al.*[19]. Please click here to view a larger version of this figure.

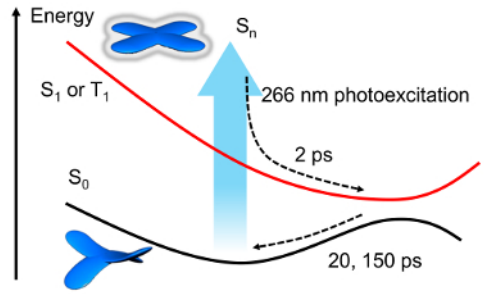

Figure 4: Schematic energy diagram of the conformational change of the π-COT core unit. The dynamical transition from a saddle (S_0) to a flat (S_1 or T_1) structure is determined from the transient transmission spectrum**.** Please click here to view a larger version of this figure.

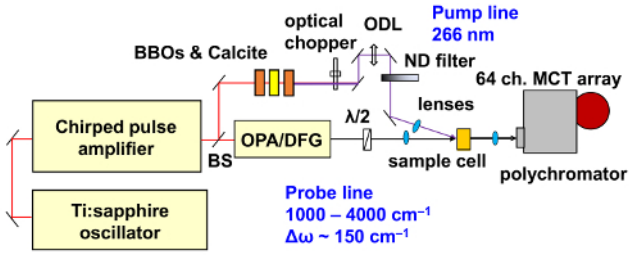

Figure 5: **Schematic diagram showing the experimental setup for time-resolved IR vibrational spectroscopy.** A Ti:sapphire oscillator generates an IR pulse with a wavelength of 800 nm, pulse duration of 120 fs, power of ~10 nJ and repetition rate of 80 MHz. A chirped pulse amplifier amplifies this pulse to a power of ~4 mJ and with a repetition rate of 1 kHz. The symbols BS, λ/2, BBOs and calcite, and ODL represent the beam splitter, λ/2 waveplate, BBO and calcite crystals and optical delay line, respectively. Please click here to view a larger version of this figure.

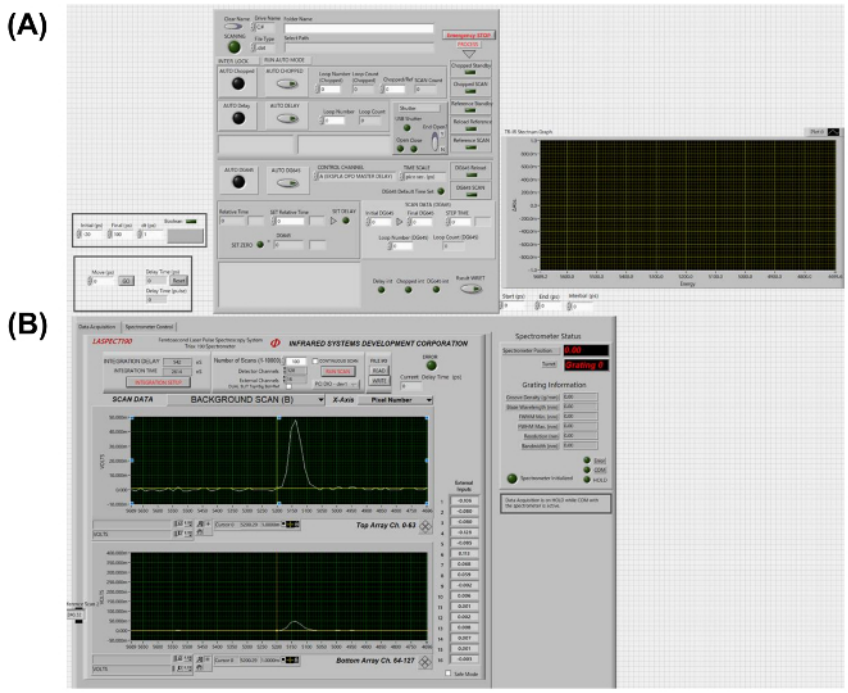

Figure 6: **Graphic user interface of the laboratory-built program for time-resolved IR vibrational spectroscopy. (A)** Setting units for the delay. **(B)** Control panels for the HgCdTe infrared spectrometer. Please click here to view a larger version of this figure.

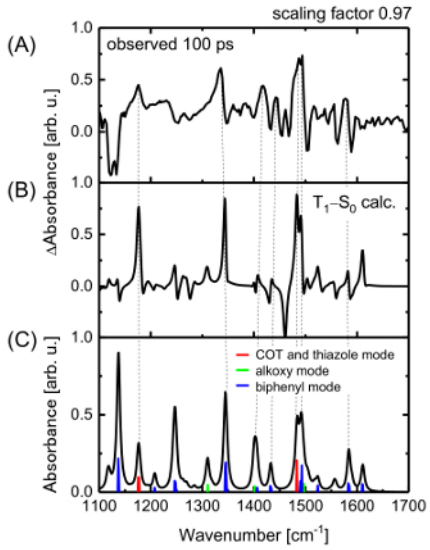

Figure 7: **Time-resolved IR spectroscopy of a π-COT-based LC thin film. (A, B)** Differential IR vibrational spectrum measured with a time delay of 100 ps compared to the calculated differential vibrational spectrum (T_1-S_0). The scaling factor for the calculated spectrum is 0.97. **(C)** Vibrational peak assignment for the T_1 spectrum. The peaks are classified as vibrational modes of the COT and thiazole rings, the alkoxy group or the biphenyl group. This figure has been adapted from Hada, M. *et al.*[19]. Please click here to view a larger version of this figure.

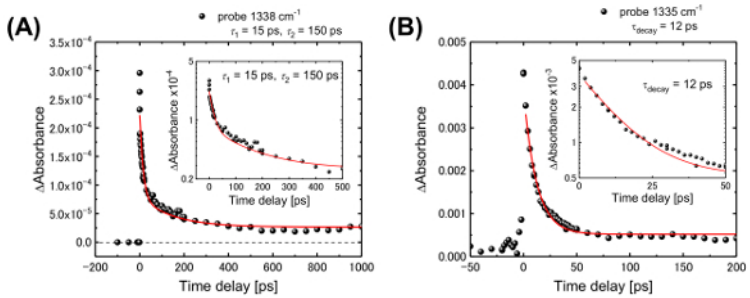

Figure 8: Time evolution of the IR peak intensity. (A) The representative wavenumbers are 1338 cm^{-1} in the LC phase and **(B)** 1335 cm^{-1} in the solution phase. The fast (20 ps) and slow (150 ps) time-constants are identical to the dynamics observed in isolated molecules and in molecules in the LC phase. The black dots and red solid lines represent the experimental data and the fitted exponential curves given by the Eq. (1), respectively. The inset of the figures represent the enlarged views of each figure withlogarithmic display. This figure has been adapted from Hada, M. *et al.*[19]. Please click here to view a larger version of this figure.

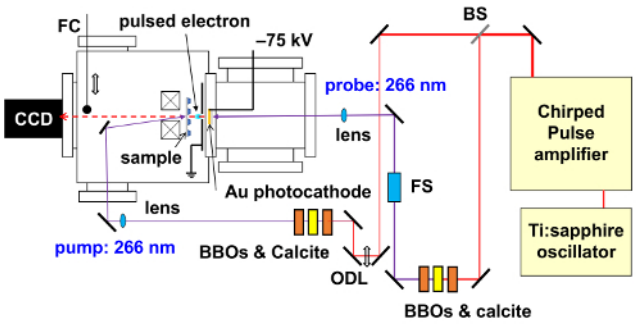

Figure 9: **Schematic illustration of the experimental setup for time-resolved electron diffraction.** A chirped pulse amplifier generates an optical pulse with a wavelength of 800 nm, pulse duration of 120 fs, power of ~2.5 mJ, and repetition rate of 1 kHz. The symbols BBOs and calcite, FS, and FC represent BBO and calcite crystals, fused silica, and faraday cap, respectively. Please click here to view a larger version of this figure.

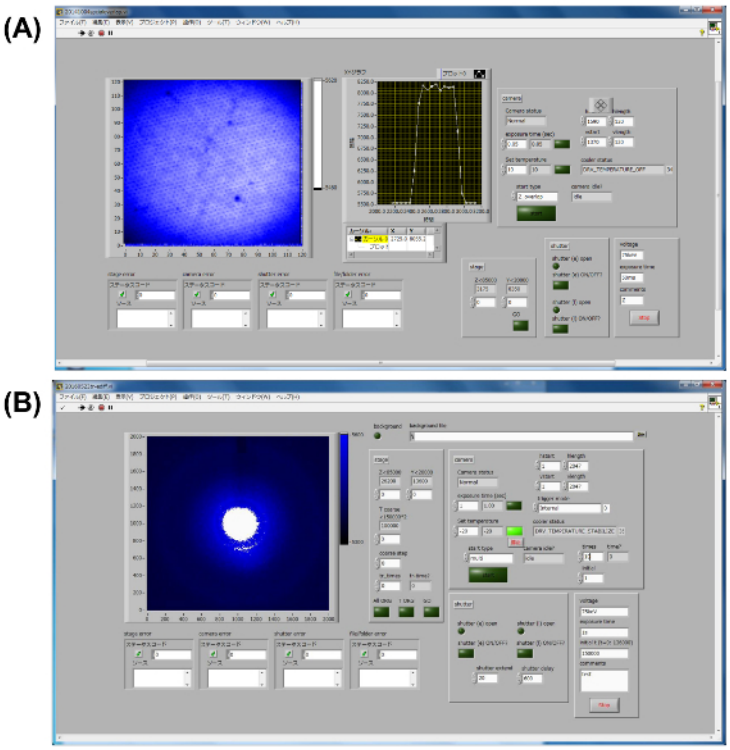

Figure 10: **Graphic user interface of the programs for the time-resolved electron diffraction. (A)** GUI for the special overlap. The image area shows the electron beam passed through the pinhole. The graphic area shows the electron beam intensity with a function of the pinhole positions. The Z-axis and Y-axis stages equipped by the sample holder (and pinhole) automatically move and the intensity of the electron beam is plotted when one selects the **Start type** as **Z_overlap** and **Y_overlap**, and then presses the **Start** button. **(B)** GUI for the time-resolved electron diffraction measurements. The image area shows electron diffraction patterns. The stage of the optical delay line automatically moves, and the electron diffraction patterns are obtained when one selects the **Start type** as **Time-resolved**, and then presses the **Start** button. Static diffraction is also obtained with selecting the **Start type** as **Single** and pressing the **Start** button. Please click here to view a larger version of this figure.

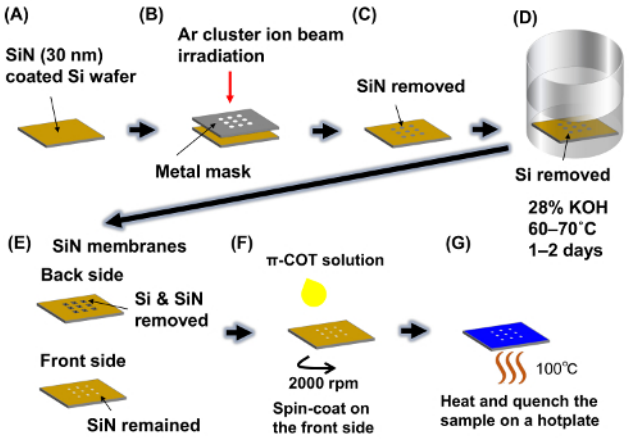

Figure 11: **Protocol to make a SiN membrane. (A)**Si wafer is coated with a SiN thin film on both sides. **(B, C)** Irradiation using an Ar cluster ion beam removes the SiN thin film on one side of the wafer. **(D)** Si etching with a KOH solution. **(E)** The SiN membrane for the sample substrate. **(F)** The sample solution is spin-coated onto the front side of the substrate. **(G)** The sample on the substrate is heated up to 100 °C and cooled down to room temperature. Please click here to view a larger version of this figure.

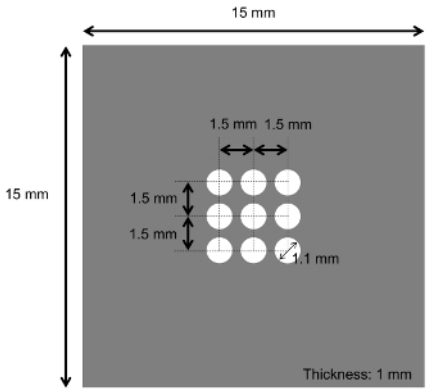

Figure 12: Design of the metal mask. The metal mask is made from stainless steel. The size of the holes (*d*: 1.1 mm) is determined by the size of the window (*w*: 0.5 mm) and the thickness of the wafer (*l*: 0.3 mm) following the equation of $d = w + 2l$. The square-shape windows can be created from the round-shape holes due to the isotropic etching of Si wafer. Please click here to view a larger version of this figure.

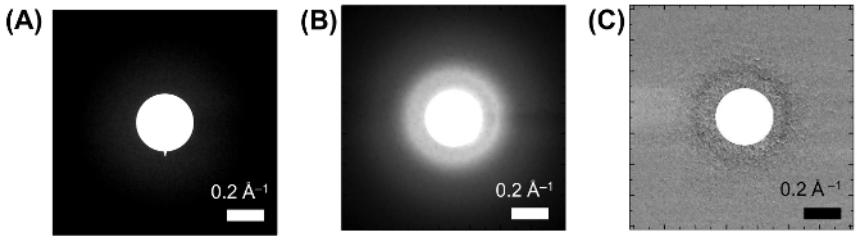

Figure 13: **Electron diffraction patterns from a π-COT-based LC thin film. (A)** The electron diffraction pattern from SiN membrane substrate. **(B)** The electron diffraction pattern from π-COT-based LC thin film without photoexcitation. **(C)** Differential diffraction pattern fromπ-COT-based LC thin film obtained with and without photoexcitation. The scale bars are the inset in the figure. Please click here to view a larger version of this figure.

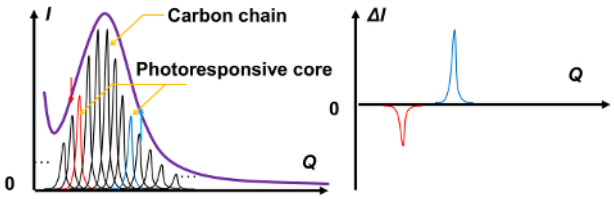

Figure 14: A schematic of the differential diffraction method. (A) The peaks from the photoresponsive moieties are buried in a broad halo pattern from the long carbon chains. **(B)** The differential diffraction method can detect the peaks from photoresponsive moieties. Please click here to view a larger version of this figure.

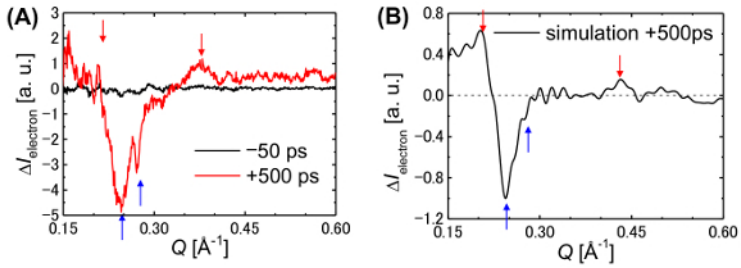

Figure 15: **Ultrafast time-resolved electron diffraction from a π-COT-based LC thin film. (A)** Differential electron diffraction pattern at -50 and 500 ps. The red and blue arrows indicate positive and negative peaks, respectively. **(B)** Simulated differential electron diffraction pattern based on an MD calculation of a columnar π-stacked structure. This figure has been adapted from Hada, M. *et al.*[19]. Please click here to view a larger version of this figure.

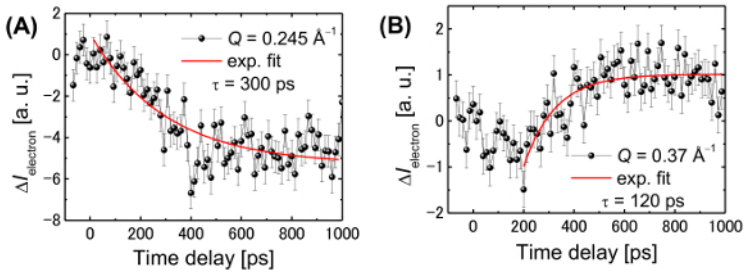

Figure 16: **Time evolution of the electron diffraction peaks. (A)** The *Q*-values of 0.245 Å^{-1} and **(B)** 0.37 Å^{-1}. Here, the *Q*-value is defined as the reciprocal number of the lattice distance (*d*). The error bars present the standard deviation of 20 measurements. This figure has been adapted from Hada, M. *et al*.[19]. Please click here to view a larger version of this figure.

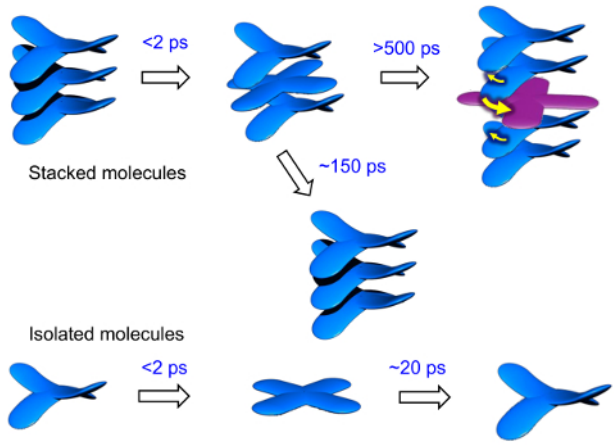

Figure 17: **Structural dynamics of the photoexcited columnar LC.** The dynamics of the columnar LC structure were observed using time-resolved IR vibrational spectroscopy and time-resolved electron diffraction. Please click here to view a larger version of this figure.

Discussion

The crucial step of the process during the time-resolved electron diffraction measurements is maintaining the high voltage (75 keV) without current fluctuation since the distance between the photocathode and anode plate is only ~10 mm. If the current fluctuates above the range of 0.1 μA before or during the experiments, increase the acceleration voltage up to 90 keV to discharge and set it again to 75 keV. This conditioning process has to be done until the current fluctuates in the range of 0.1 μA. The proper design of the electron source with enough dielectric strength is the most important point to develop this kind of machine.

In general, time-resolved IR vibrational spectroscopy and time-resolved electron diffraction techniques can be applied for only the materials that undergo photoinduced structural changes. However, these techniques have great advantages to observe the structural dynamics on soft materials because the electron probe is more sensitive to the positions of light elements (carbon, oxygen, nitrogen, hydrogen, *etc*.) than the X-ray probes, and because the mid-IR probe is more sensitive to the vibrational mode of the bonds between the light elements than the light with other range of wavelength.

In summary, differential-detection analyses of the combination of time-resolved IR vibrational spectroscopy and electron diffractometry can provide direct observations of the structures and the dynamics of LC materials. This approach can be applied more generally to determine the local structural motions of stimuli-responsive units in complicated soft matter systems, such as cell-membrane proteins, suggesting a new direction for the science of ultrafast structural dynamics.

Disclosures

The authors have nothing to disclose.

Acknowledgements

We thank Dr. S. Tanaka at Tokyo Institute of Technology for time-resolved IR vibrational spectroscopy measurements and Prof. M. Hara and Dr. K. Matsuo at Nagoya University for XRD measurements. We also thanks Prof. S. Yamaguchi at Nagoya University, Prof. R. Herges at Kiel University and Prof. R. J. D. Miller at the Max Planck Institute for the Structure and Dynamics of Matter for valuable discussion.

This work is supported by the Japanese Science Technology (JST), PRESTO, for funding the projects "Molecular technology and creation of new functions" (Grant Number of JPMJPR13KD, JPMJPR12K5, and JPMJPR16P6) and "Chemical conversion of light energy". This work is also partially supported by JSPS Grant Numbers JP15H02103, JP17K17893, JP15H05482, JP17H05258, JP26107004, and JP17H06375.

References

1. Van Haaren, J., Broer, D. In search of the perfect image. *Chem. Ind.* **24**, 1017-1021 (1998).
2. Goodby, J.W., Collings, P.J., Kato, T., Tschierske, C., Gleeson H.F., Raynes, P., Eds. *Handbook of Liquid Crystals.* Wiley-VCH. Weinheim. (2014).
3. Li, Q. Ed. *Liquid Crystal Beyond Displays.* John Wiely & Sons. Hoboken. (2012).
4. Kato, T.Self-assembly of phase-segregated liquid crystal structures. *Science.* **295**, 2414-2418 (2002).
5. Fleismann, E.K., Zentel, R.Liquid-Crystalline Ordering as a Concept in Materials Science: From Semiconductors to Stimuli-Responsive Devices. *Angew. Chem. Int. Ed.* **52**, 8810-8827 (2013).
6. Sergeyev, S., Pisula, W., Geerts, Y.H.,Discotic liquid crystals: a new generation of organic semiconductors. *Chem. Soc. Rev.* **36**, 1902-1929 (2007).
7. Goodby, J.W.Mesogenic molecular crystalline materials. *Curr. Opin. Solid State Mater. Sci.* **4**, 361-368 (1999).
8. Ichimura, K.,Photoalignment of Liquid-Crystal Systems. *Chemical Reviews.* **100**, 1847-1873 (2000).
9. Ikeda, T.,Photomodulation of liquid crystal orientations for photonic applications. *J. Mater. Chem.* **13**, 2037-2057 (2003).
10. Browne, W.R., Feringa, B.L.Making molecular machines work. *Nat. Nanotech.* **1**, 25-35 (2006).
11. Ikeda, T., Mamiya, J., Yu, Y.Photomechanics of liquid-crystalline elastomers and other polymers. *Angew. Chem., Int. Ed.* **46**, 506−528 (2007).
12. Sagara, Y., Kato, T.Brightly Tricolored Mechanochromic Luminescence from a Single-Luminophore Liquid Crystal: Reversible Writing and Erasing of Images. *Angew. Chem. Int. Ed.* **50**, 9128-9132 (2011).
13. Miyajima, D. *et al.*Ferroelectric columnar liquid crystal featuring confined polar groups within core-shell architecture. *Science.* **336**, 209-213 (2012).
14. White, T.J., Broer, D.J.Programmable and adaptive mechanics with liquid crystal polymer networks and elastomers. *Nat. Mater.* **14**, 1087−1098 (2015).
15. Saito, S. *et al.* Light-melt adhesive based on dynamic carbon frameworks in a columnar liquid-crystal phase. *Nat. Commun.* **7**, 12094 (2016).
16. Lagerwall, J.P.F., Giesselmann, F.Current Topics in Smectic Liquid Crystal Research. *Chem. Phys. Chem.* **7**, 20-45 (2006).
17. Yoon, H.G., Agra-Kooijman, D.M., Ayub, K., Lemieux, R.P., Kumar, S. Direct Observation of Diffuse Cone Behavior in de Vries Smectic-A and -C Phases of Organosiloxane Mesogens. *Phys. Rev. Lett.* **106**, 087801 (2011).
18. Takanishi, Y., Ohtsuka, Y., Takahashi, Y., Kang, S., Iida, A. Chiral doping effect in the B2 phase of a bent-core liquid crystal: The observation of resonant X-ray satellite peaks assigned to the 5/10 layer periodic structure. *Euro. Phys. Lett.* **109**, 56003 (2015).
19. Hada, M. *et al.*Structural Monitoring of the Onset of Excited-State Aromaticity in a Liquid Crystal Phase. *J. Am. Chem. Soc.* **139**, 15792-15800 (2017).
20. Cavalleri, A. *et al.*Femtosecond Structural Dynamics in VO_2 during an Ultrafast Solid-Solid Phase Transition. *Phys. Rev. Lett.* **87**, 237401 (2001).
21. Hada, M., Okimura, K., Matsuo, J.Characterization of structural dynamics of VO_2 thin film on c-Al_2O_3 using in-air time-resolved x-ray diffraction. *Phys. Rev. B.* **82**, 153401 (2010).
22. Eichberger, M. *et al.*Snapshots of cooperative atomic motions in the optical suppression of charge density waves. *Nature.* **468**, 799-802 (2010).
23. Ichikawa, H. *et al.* Transient photoinduced 'hidden' phase in a manganite. *Nat. Mater.* **10**, 101-105 (2011).
24. Hada, M., Okimura, K., Matsuo, J. Photo-induced lattice softening of excited-state VO_2. *Appl. Phys. Lett.* **99**, 051903 (2011).
25. Zamponi, F., Rothhardt, P., Stingl, J., Woerner, M., Elsaesser, T.Ultrafast large-amplitude relocation of electronic charge in ionic crystals. *P. Natl. Acad. Sci. USA.* **109**, 5207-5212 (2012).
26. Beaud, P. *et al.*A time-dependent order parameter for ultrafast photoinduced phase transitions. *Nat. Mater.* **13**, 923-927 (2014).
27. Morrison, V.R. *et al.*A photoinduced metal-like phase of monoclinic VO# revealed by ultrafast electron diffraction. *Science.* **346**, 445-448 (2014).
28. Han, T.-R. T. *et al.*Exploration of metastability and hidden phases in correlated electron crystals visualized by femtosecond optical doping and electron crystallography. *Sci. Adv.* **5**, e1400173 (2015).
29. Waldecker, L. *et al.*Time-domain separation of optical properties from structural transitions in resonantly bonded materials. *Nat. Mater.* **14**, 991-995 (2015).
30. Minitti, M.P. *et al.*,Imaging Molecular Motion: Femtosecond X-Ray Scattering of an Electrocyclic Chemical Reaction. *Phys Rev. Lett.* **114**, 255501 (2015).
31. Kim, K.H. *et al.*,.Direct observation of bond formation in solution with femtosecond X-ray scattering. *Nature.* **518**, 385-389 (2015).
32. Gao, M. *et al.*Mapping molecular motions leading to charge delocalization with ultrabright electrons. *Nature.* **496**, 343-346 (2013).
33. Ishikawa, T. *et al.*, Direct observation of collective modes coupled to molecular orbital-driven charge transfer. *Science.* **350**, 1501-1505 (2015).
34. Xian, R. *et al.*,Coherent ultrafast lattice-directed reaction dynamics of triiodide anion photodissociation. *Nat. Chem.* **9**, 516-522 (2017).
35. Chapman, H.N. *et al.*,Femtosecond X-ray protein nanocrystallography. *Nature.* **470**, 73-77 (2011).
36. Ishikawa, T. *et al.* A compact X-ray free-electron laser emitting in the sub-ångström region. *Nature Photonics.* **6**, 540-544 (2012).
37. Zewail, A.H. Four-dimensional electron microscopy. *Science.* **328**, 187-193 (2010).
38. Sciaini, G., Miller, R.J.D.Femtosecond electron diffraction: heralding the era of atomically resolved dynamics. *Rep. Prog. Phys.* **74**, 096101 (2011).
39. Hada, M., Pichugin, K., Sciaini, G.Ultrafast structural dynamics with table top femtosecond hard X-ray and electron diffraction setups. *Euro. Phys. J. Special Topic.* **222**, 1093-1123 (2013).
40. Miller, R.J.D. Mapping atomic motions with ultrabright electrons: the chemists' gedanken experiment enters the lab frame. *Annu. Rev. Phys. Chem.* **65**, 583-604 (2014).

41. Seki, T., Murase, T., Matsuo, J.Cluster size dependence of sputtering yield by cluster ion beam irradiation. *Nucl. Instrum. Methods Phys. Res. B.* **242**, 179-181 (2006).
42. Mueller, C., Harb, M., Dwyer, J.R., Miller, R.J.D.Nanofluidic Cells with Controlled Pathlength and Liquid Flow for Rapid, High-Resolution In Situ Imaging with Electrons. *J. Phys. Chem. Lett.* **4**, 2339-2347 (2013).
43. Mouri, K., Saito, S., Yamaguchi, S. Highly Flexible π-Expanded Cyclooctatetraenes: Cyclic Thiazole Tetramers with Head-to-Tail Connection. *Angew. Chem. Int. Ed.* **51**, 5971-5975 (2012).
44. Mouri, K., Saito, S., Hisaki, I., Yamaguchi, S. Thermal 8π electrocyclic reaction of heteroarene tetramers: new efficient access to π-extended cyclooctatetraenes. *Chem. Sci.* **4**, 4465-4469 (2013).
45. Rosenberg, M., Dahlstrand, C., Kilså, K., Ottosson, H.Excited State Aromaticity and Antiaromaticity: Opportunities for Photophysical and Photochemical Rationalizations. *Chem. Rev.* **114**, 5379-5425 (2014).
46. Kato, T., Mizoshita, N., Kishimoto, K.Functional Liquid-Crystalline Assemblies: Self-Organized Soft Materials. *Angew. Chem. Int. Ed.* **45**, 38-68 (2006).
47. Rosen, B.M. *et al.*, Dendron-Mediated Self-Assembly, Disassembly, and Self-Organization of Complex Systems. *Chem. Rev.* **109**, 6275-6540 (2009).
48. Fukazawa, N. *et al.*Time-Resolved Infrared Vibrational Spectroscopy of the Photoinduced Phase Transition of $Pd(dmit)_2$ Salts Having Different Orders of Phase Transition. *J. Phys. Chem. C.* **117**, 13187 (2013).
49. Mukuta, T. *et al.*Infrared Vibrational Spectroscopy of $[Ru(bpy)_2(bpm)]^{2+}$ and $[Ru(bpy)_3]^{2+}$ in the Excited Triplet State. *Inorg. Chem.* **53**, 2481-2490 (2014).
50. Tanaka, S., Takahashi, K., Hirahara, M., Yagi, M., Onda, K. Characterization of the excited states of *distal-*. and *proximal-*.$[Ru(tpy)(pynp)OH_2]^{2+}$ in aqueous solution using time-resolved infrared spectroscopy. *J. Photochem. Photobio. A.* **313**, 87-98 (2015).
51. Mukuta, T., Tanaka, S., Inagaki, A., Koshihara, S., Onda, K.Direct Observation of the Triplet Metal-Centered State in $[Ru(bpy)_3]^{2+}$ Using Time-Resolved Infrared Spectroscopy. *ChemistrySelect.* **1**, 2802-2807 (2016).
52. Epp, S.W. *et al.* Time zero determination for FEL pump-probe studies based on ultrafast melting of bismuth. *Str. Dyn.* **4**, 054308 (2017).
53. Hada, M. *et al.* Cold ablation driven by localized forces in alkali halides. *Nat. Commun.* **5**, 3863 (2014).
54. Hada, M. *et al.*Ultrafast time-resolved electron diffraction revealing the nonthermal dynamics of near-UV photoexcitation-induced amorphization in $Ge_2Sb_2Te_5$. *Sci. Rep.* **5**, 13530 (2015).
55. Hada, M. *et al.*Evaluation of Damage Layer in an Organic Film with Irradiation of Energetic Ion Beams. *Jpn. J. Appl. Phys.* **49**, 036503 (2010).
56. Hada, M. *et al.*Bandgap modulation in photoexcited topological insulator Bi_2Te_3 via atomic displacements. *J. Chem. Phys.* **145**, 024504 (2016).
57. Manz, S. *et al.* Mapping atomic motions with ultrabright electrons: towards fundamental limits in space-time resolution. *Faraday Discuss.* **77**, 467-491 (2015).

